LA-UR- 09-01279

Approved for public release;
distribution is unlimited.

Title:	Dynamic Shear Deformation in High Purity Iron
Author(s):	E.K. Cerreta (MST-8) J.F. Bingert (MST-8) C.P. Trujillo (MST-8) M.F. Lopez (MST-8) G.T. Gray III (MST-8)
Intended for:	DYMAT 2009 September 7-11, 2009 Brussels, Belgium

Form 836 (7/06)

Dynamic Shear Deformation in High Purity Iron

E.K. Cerreta[1], J.F. Bingert[1], C.P. Trujillo[1], M.F. Lopez[1], and G.T. Gray[1]

[1]*Los Alamos National Laboratory, MST-8/MS G755, Los Alamos, NM 87545 USA*

Abstract. The forced shear test specimen first developed Meyer and Manwarring [1] has been utilized in a number of studies. While the geometry of this specimen does not allow for the microstructure to determine location of shear band formation and the overall mechanical response of a specimen is highly sensitive to the exact geometry utilized, the forced shear specimen is useful for characterizing the influence of parameters such strain rate, temperature, strain, and load on the microstructural evolution within a shear band. Additionally, many studies have utilized this geometry to advance the understanding of shear band development. In this study, by varying the geometry, specifically the ratio of the inner hole diameter to the outer hat diameter, the dynamic shear localization response of high purity Fe is examined. Post mortem characterization was performed to quantify the width of the localizations and to examine the microstructural and textural evolution of shear deformation in a bcc metal. Increased instability in mechanical response is strongly linked with development of enhanced intergranular misorientations, high angle boundary development, and well developed classical shear textures characterized through orientation distribution functions.

1. INTRODUCTION

Shear deformation and failure is significant to multiple applications ranging from metal cutting operations involving high rates of deformation to dynamic loading environments such as auto impacts and ballistic scenarios[2, 3]. In many shear loading environments failure is preceded by shear localization or banding. Shear band formation is typically enhanced at high strain rates because lack of time for heat diffusion is considered to lead to non-uniform strain [3]. Adiabatic shear banding is one of the best known examples of plastic flow localization due to thermal softening. This phenomenon, first observed by Zener and Hollman, is termed adiabatic because of the short time scales involved with potentially large temperature increases[4]. A great deal of research has focused on the properties of shear localization and banding because it has been shown to be a precursor to failure in many metals.

Research on shear banding has typically focused on two specific areas of study: (1) modeling descriptions and criteria development for plastic flow instability and (2) the relationship of shear banding to initial microstructure. In shear deformed metals, many microstructural alterations have been observed. These include: dynamic recovery, dynamic recrystallization, phase transformations, melting, and amorphization [5, 6]. Recent studies have focused on correlating evolving microstructure and mechanical response during shear localization. Mechanisms that control substructures within shear bands appear to be strongly related to initial microstructure, its evolution, and therefore its work hardening capability [7-9]. Additionally, while the current understanding of the influence of texture on shear banding is limited, it has been shown that some grains with preferred orientations might be favorable for the formation of shear bands [10].

A sample geometry that has been utilized to probe the influence of microstructure, strain rate, and temperature on the evolution of a shear localization is the forced shear or 'tophat' specimen. It is

an axi-symmetric sample with an upper hat portion, a lower brim portion, and a shear section between the hat and brim sections. The geometry was originally designed by Meyer and Manwarring [1] but has been modified several times within the literature. This general specimen geometry defines the location of localization and shear band formation making it inappropriate for studying shear band initiation but ideal for studying evolution and growth because the difficult problem of identifying points of shear band initiation within a specimen exposed to general loading is alleviated [11].

In this study, the geometry of the forced shear specimen is altered systematically as shown in Fig. 1, to examine the influence of the combined shear - compression loading geometry of the forced shear specimen on microstuctural evolution during dynamic loading. Post mortem characterization, both optical and electron microscopy techniques, was performed to quantify damage in the localization regions and examine the textural evolution of shear deformation. Increased instability in mechanical response observed as the geometry approaches a pure shear loading configuration, is strongly linked with development of enhanced intergranular misorientations, high angle boundary development, and well developed classical shear textures characterized through both pole figures (pf) and orientation distribution functions (odf).

2. EXPERIMENTAL

The polycrystalline Fe used in this study was electrical grade, hot finish, high-purity iron supplied as a 12cm x 12cm billet. The chemistry is given in Table 1and the average equiaxed grain size is 60μm. The crystallographic texture of the high purity Fe in this study was characterized using X-ray diffraction. The odf texture strength for the high purity wrought iron was measured to be 1.25, indicative of a nearly random polycrystalline solid [12]. Tophat specimens in the geometries shown in Fig. 1 were machined from the as received metal. From this figure, it can be seen that the state of shear changes from one that is a combined loading state of shear and compression, because the inner hole diameter of the brim is smaller than the outer hat diameter, to an almost pure shear loading geometry, where the inner hole diameter of the brim is nearly equal to the outer hat diameter. This evolution of specimen geometry is expected to cause a significant difference in the evolved shear localization structure and to understand the extent of this difference, the Fe specimens were dynamically loaded on a Split Hopkinson Pressure Bar. Post mortem specimens were characterized both optically and with electron back scattered diffraction (EBSD) to quantify differences in shear localization evolution based on specimen geometry. Specimens in each of the geometries shown in Fig.1 were loaded at 3100/s and 298K to total displacements between 0.27 and 0.35mm.

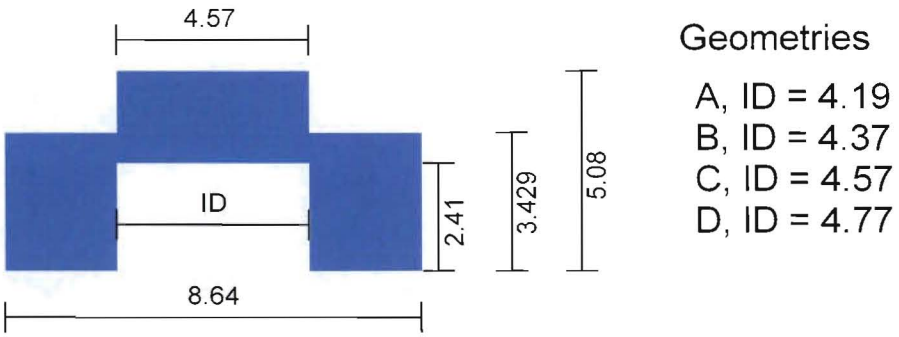

Figure 1. The general tophat geometry and modification of this geometry for A, B, C, and D geometries in mm.

Table 1. Chemical Analysis of Fe (in ppm wt%)

C	Mn	Si	P	S	Cr	Ni	Fe
0.013	0.10	0.14	0.005	0.010	0.16	0.13	Bal.

Each of these specimens was then cross sectioned parallel to the loading axis, mounted, and polished for post mortem characterization. Specimens were ground to 1μm Alumina and then etched with Nital. The cross sectioned specimens resemble the schematic in Fig. 1 and therefore two shear affected zones (SAZ's) can be viewed in each specimen.

3. RESULTS

The mechanical test data for these tests is plotted engineering shear stress vs. displacement in Fig. 2. The flow stresses and rates of work hardening decreased as the inner-hole diameter (dimension ID in Fig. 1) increases. For the largest diameters (C and D), the work hardening rate is decreasing and indicative of significant shear deformation. The relatively higher rates of work hardening in specimens A and B are indicative of more stable deformation and the combined loading state in the gauge section of these specimens, shear and compression. This is due to forcing a larger diameter hat through a smaller diameter inner hole. A hoop stress is exerted by the brim on the gauge section creating a compressive component to the test.

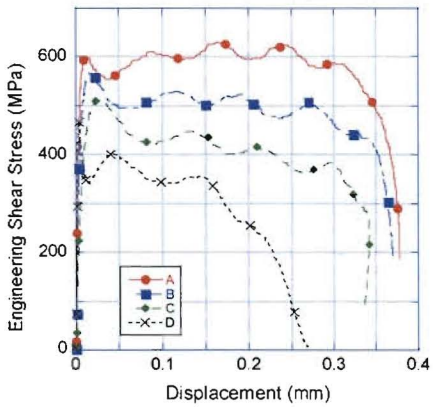

Figure 2. Engineering Shear Stress vs. Displacement data for each of the geometries tested.

Post mortem analysis of the shear deformed zones revealed that in all cases no shear band was formed but rather a region of localized plastic deformation developed in which grains in the gauge section of the tested tophat specimens had elongated in the direction of shear deformation, Fig. 3. To quantify the extent of these damage regions, intergranular misorientation deviation (IMD) maps of the plastically deformed regions were calculated. These maps measure the average of all deviations between each point in a grain and the grain's average orientation. From these maps, Fig. 4, widths of the shear localized regions can be measured. This measurement is the average of five measurements of the width of the shear localized zone, determined by the boundary created by the light gray grains in each map. These calculated widths are in Table 2. The width of the shear localized regions decreases from A to B to C geometries and then slightly increases with D geometry. This correlates with the high degree of microstructural localization expected in the geometry closest to a pure shear loading configuration, geometry C.

Table 2. Widths if the Shear Localized Region (μm)

Geometry	A	B	C	D
Width	228	203	192	207

In addition to the quantification of the widths, the low (0-10°) and high angle boundary (10-62.5°) distributions and the texture development within the shear localized zones have been examined.

Figure 5 gives the low (LAB) and high (HAB) angle boundary percentages for the shear localized regions for each tested geometry. It can be seen from this data that the HAB percentage steadily increases as the geometry approaches a pure shear loading configuration (A to C) and then decreases slightly with the D geometry. Deformation texture development was also examined in the Fe tophat samples as a function of specimen geometry, Fig. 6. For each EBSD data set, the central SAZ was cropped so as to eliminate regions that may have experienced only modest shear strains. Within this heavily strained region, orientations with confidence indices < 0.001 were not considered. This led to a reduction of no more than 10% of orientations within the cropped region. Orientation data were rotated so as to align the shear direction (SD) with the horizontal axis and the shear plane normal (SP) with the vertical axis. While shear texture evolution in bcc metals has received significantly less attention than for fcc metals, shear textures can be defined by {hkl}<uvw> associated with the {SP} <SD> sample reference frame [13]. The primary bcc fibers are {110}//SP and <111>//SD. 110 and 111 pf's recalculated from the odf are shown in Fig. 6. The pf's qualitatively appeared to contain features expected for bcc shear textures, but did not represent ideal shear textures.

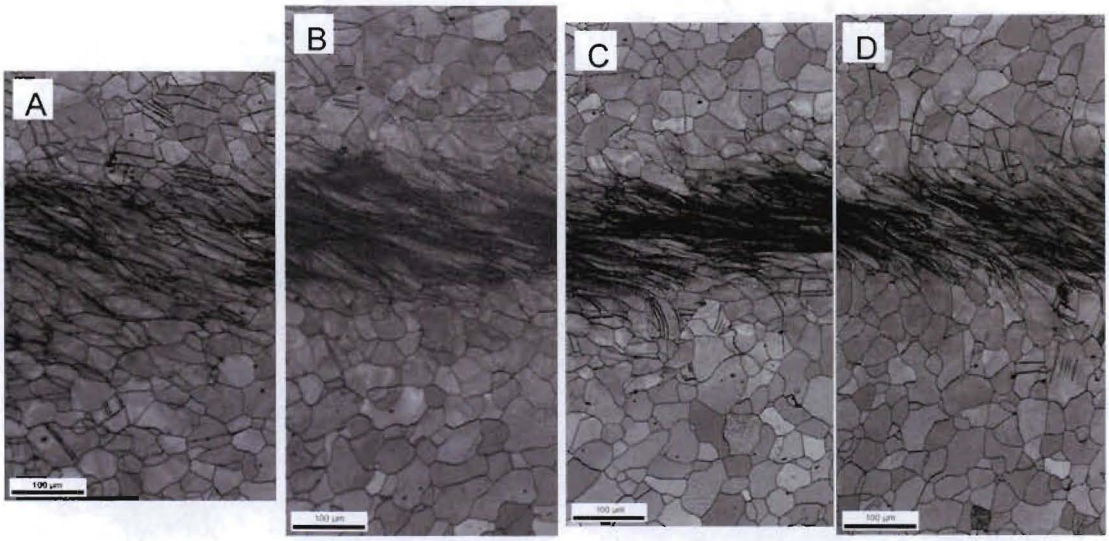

Figure 3. Image quality maps of the shear deformed regions in the specimens with A through D geometries.

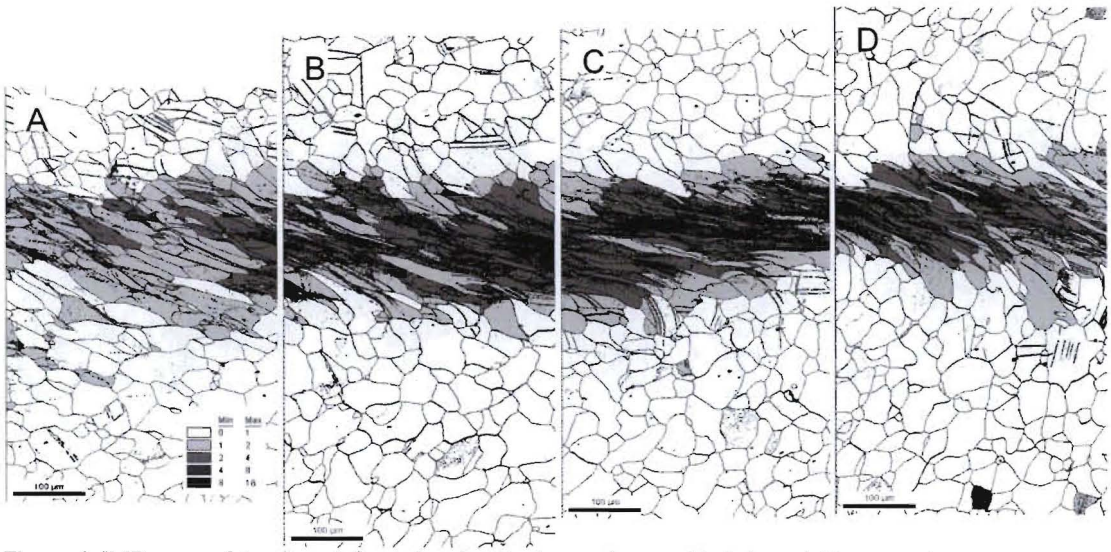

Figure 4. IMD maps of the shear deformed regions in the specimens with A through D geometries.

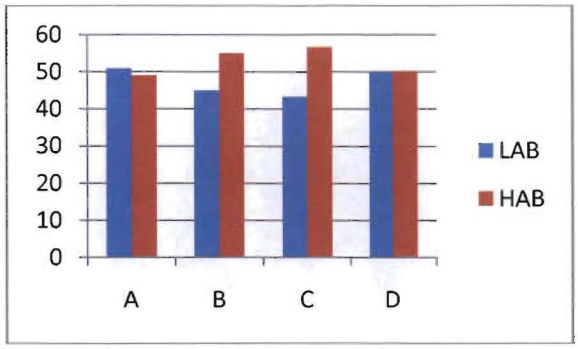

Figure 5. LAB and HAB fractions as a function of geometry.

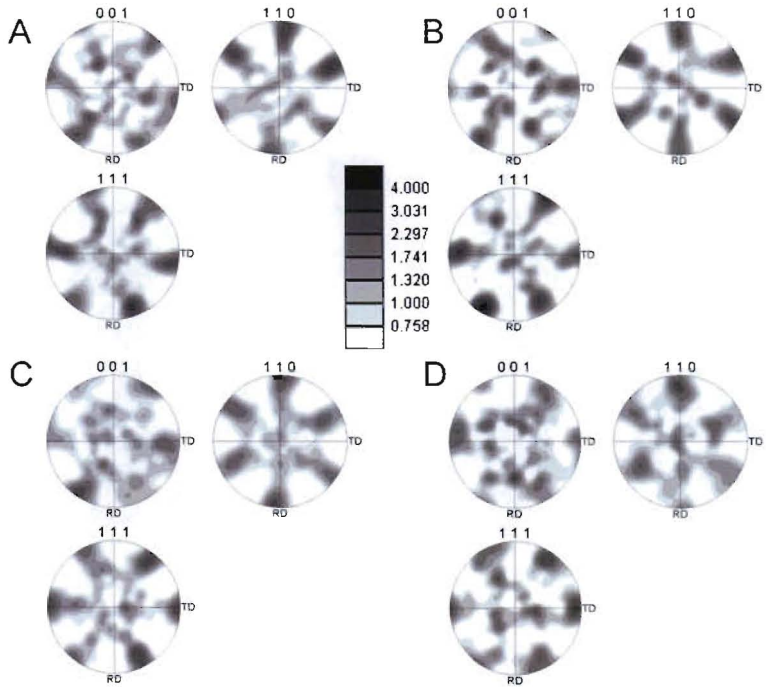

Figure 6. Deformation texture development as a function of geometry.

4. DISCUSSION AND CONCLUSIONS

The mechanical response, Fig. 2, was highly dependent upon specimen geometry. Both the flow stresses and rates of work hardening were higher for the A and B geometries as compared to the C and D geometries. This is attributed to differences in the loading configuration (shear-compression) as a function of geometry, Fig. 1. Clearly, as a pure shear loading configuration is approached instability in mechanical response is promoted. Considère criterion, originally developed to predict necking during tensile tests, states that mechanical instability is linked to work hardening [14, 15]. The microstructural evolution reflected this effect. The narrowest region of shear localization, highest fractions of HABs, and most well developed shear textures were observed for the C-geometry.

Based on the observed microstructures in this study and the mechanical response, Figs. 2-4, as well as the observations of shear deformation in Ta and Cu, it is clear that the specimen geometry influences the dislocation generation, glide and storage phenomena that control shear deformation in Fe [9, 16]. Additionally the development of an increasing density of high angle boundaries, Fig. 5, is important to accommodation of increasing degrees of shear deformation.

A subgrain rotation model called PriSM (progressive subgrain misorientation) was proposed to account for high angle dynamically recrystallized structures observed during dynamic mechanical deformation [17]. While here, not enough high resolution microstructural analysis has been performed to determine the true nature of the subgrain development in the shear localized regions - recrystallized or not - the development of the HAB fraction as a function of geometry is consistent with the substructural evolution model described in the PriSM model.

In summary, varying the inner diameter of the tophat specimen changes the shear-compression loading state which in turn significantly influences the mechanical response and the microstructural evolution during deformation. More localized shear deformation, higher fractions of high angle boundaries, and a more well developed shear texture are all observed as the loading state approaches pure shear loading. This correlates well with decreasing work rates observed as a function of geometry, A-D, and indicates that mechanical subgrain rotation is likely accommodating shear deformation.

Acknowledgments
This work has been performed under the auspices of the United States Department of Energy.

References
[1] Meyer, L. W. and Manwarring, S., "Critical Adiabatic Shear Strength of Low Alloyed Steel Under Compressive Loading", in Metallurgical Applications of Shock Wave and High Strain Rate Phenomena, Murr, L. E., Staudhammer, K. P. and Meyers, M., eds., Marcel Decker, vol. 1986, pp. 657.
[2] Semiatin, S. L., Staker, M. A. and Jonas, J. J., *Acta Metal.*, **32** (1984) 1347-1354.
[3] Clifton, R. J., Duffy, J., Hartley, K. A. and Shawki, T. G., *Scripta Metal.*, **18** (1984) 443-448.
[4] Rittel, D., Wang, Z. G. and Merzer, M., *Physical Review Letters*, **96** (2006) 075502-1-4.
[5] Meyers, M. A., Xu, Y. B., Xue, Q., Perez-Prado, M. T. and McNelley, T. R., *Acta Mater.*, **51** (2003) 1307.
[6] Xue, Q., Meyers, M. and Nesterenko, V. F., *Acta Mater.*, **50** (2002) 575-596.
[7] Xue, Q. and Gray, G. T., *Metal. Mater. Trans. A*, **37** (2006) 2435-2446.
[8] Xue, Q. and Gray, G. T., *Metal. Mater. Trans. A*, **37** (2006) 2447-2458.
[9] Dougherty, L. M., Cerreta, E. K., Pfeif, E. A., Trujillo, C. P. and Gray III, G. T., *Acta Mater.*, **55** (2007) 6356-64.
[10] Xue, Q., Bingert, J. F., Henrie, B. L. and Gray III, G. T., *Mat. Sci. Eng. A*, **473** (2008) 279-289.
[11] Bronkhorst, C., Cerreta, E., Xue, Q., Maudlin, P. J., Mason, T. A. and Gray III, G. T., *Int. J. Plas.*, **22** (2006) 1304-1335.
[12] Gray, G., Hayes, D. and Hixson, R., *J. de Phys IV:6th International Conference on Mechanical and Physical Behaviour of Materials Under Dynamic Loading*, **10** (2000) 755-760.
[13] Bingert, J. F., Livescu, V. and Cerreta, E. K., "Characterization of Shear Localization and Shock Damage", in Electron Backscatter Diffraction in Materials Science, Schwartz, A. J., eds., Springer Science, vol. 2009, in press.
[14] Recht, R. F., *J. Appl. Mech.*, **31** (1964) 189-193.
[15] Reed-Hill, R. E. and Abbaschian, R., in Physical Metallurgy Principles, PWS Publishing Company, Boston, 1994, pp.
[16] Cerreta, E. K., Frank, I. J., Gray III, G. T., Trujillo, C. P., Korzekwa, D. A. and Dougherty, L. M., *Mat. Sci. Eng. A*, **501** (2009) 207-219.
[17] Hines, J. A., Vecchio, K. S. and Ahzi, S., *Metal. Mater. Trans. A*, **29** (1998) 191-203.